Drift Alfvén Energetic Particle Stability with Circulating Particles

Y. Li[1], S. Hu[2], W. Zheng[3], Y. Xiao[1*]

[1] Institute for Fusion Theory and Simulation and Department of Physics, Zhejiang University, Hangzhou, 310027, PRC

[2] College of Physics, Guizhou University, Guiyang, PRC

[3] Academy of Mathematics and Systems Science, Chinese Academy of Sciences

* (Corresponding author) E-mail: yxiao@zju.edu.cn

Abstract

We develop from scratch a comprehensive linear stability eigenvalue code based on finite element method (FEM), namely the Drift Alfvén Energetic Particle Stability (DAEPS) code, to investigate the most unstable or stable dangerous modes widely observed in toroidal fusion plasmas. The DAEPS code is dedicated to providing a thorough understanding of marginally unstable low frequency mode physics in collisionless plasmas, e.g., shear Alfvén wave (SAW) and drift Alfvén wave (DAW) physics with energetic particle (EP) effect. DAEPS can calculate the linear frequency and growth rate for these modes by keeping correct asymptotic behavior in ballooning space. In this work, we demonstrate that the DAEPS code is able to analyze linear electromagnetic modes excited by circulating particles, including thermal particle excited BAE and EP excited TAE which are successfully benchmarked with other codes and theories, where the finite orbit width is discovered to play an important stabilizing role which are usually ignored by traditional theory.

I. Introduction

Tokamak experiments observe that energetic particles (EPs) can resonantly destabilize various Alfvén eigenmodes (AEs) [1-6]. These Alfvénic fluctuations, which are marginally unstable or weakly damped in the presence of EP, have been shown to eject a large number of resonant EPs from the core plasma [1, 3, 5, 7]. These observed

Alfvénic fluctuations are caused by various instabilities excited by EPs, which consist of beta-induced Alfvén eigenmode (BAE) [8], toroidicity-induced Alfvén eigenmode (TAE) [9], energetic particle mode (EPM) [10], reversed shear Alfvén eigenmode (RSAE) [11], etc. Some of these instabilities are primarily related to the parallel dynamics of circulating EPs [12], while some are related to the precessional dynamics of trapped EPs [13]. The EP heat and particle loss caused by these Alfvén eigenmodes will pose a grand challenge for approaching and sustaining the ignition condition for future fusion reactors including ITER, as well as a stringent constraint for the lifetime of the wall material that is bombarded continuously by this high power EP flux [12, 14]. Therefore, it is important to fully understand the AE physics and develop effective methods to regulate the AE induced EP transport.

In the last decades, lots of theoretical [9, 15-17] efforts have been made to understand the AE physics. The linear and nonlinear properties of AEs have also been widely studied by the numerical simulation using MHD-kinetic hybrid codes [3, 18-22] and gyrokinetic codes [4, 6, 23, 24]. In the numerical investigation of the Alfvénic instabilities, the ballooning representation is widely employed by various numerical codes [7, 25-28]. However, the boundary condition (BC) implemented in these numerical codes usually set the fluctuating field $\delta\psi \to 0$ as the extended poloidal angle of the ballooning representation in the computational boundary [7, 25-28], which cannot accurately represent the asymptotic behavior of the mode structure for most interesting cases. The inaccuracy of the asymptotic behavior will cause even larger errors in calculating frequency and growth rate for marginally unstable or damping modes, and large deviations from the actual mode structure in the inertial region. Thus, the unphysical boundary conditions implemented in the numerical codes will lead to inaccuracy in computing the potential energy and misinterpretation of the AE physics.

The hybrid MHD-kinetic model extensively used to study EP induced Alfvénic instabilities consists of two approaches, namely perturbative approach and non-perturbative approach [21]. In the perturbative approach, the eigen frequency and the mode structure are calculated from the MHD equation, which are then used to calculate

the kinetic response and the kinetic potential energy δW_k. This kinetic energy transferring from the EP to the mode is then used to calculate the linear growth rate. Another approach, the non-perturbative approach includes the EP contribution through the plasma pressure or current perturbation, whose mode structure and eigen frequency differ from those from the MHD equation in many important circumstances. The perturbative approach cannot be applied to the EPM, since the mode doesn't exist in the MHD framework and is very sensitive to the EP source [10, 29].

In this paper, we develop a non-perturbative eigenvalue code called Drift Alfvén Energetic Particle Stability code, which uses the finite element method (FEM) to self-consistently solve the eigen frequency and growth rate, as well as the asymptotic behavior in the inertial region. This code is benchmarked on various instabilities involving circulating particle dynamics with other codes and theories. The importance of the finite Larmor radius effect (FLR) and finite orbit width effect (FOW) is discovered in the code verification process.

The paper is organized as follows. In Section II, we introduce the model equations of the DAEPS code. In Section III, the numerical method used in DAEPS is discussed in details. Then we use the DAEPS to study the linear physics of BAE/KBM and benchmark these physics issues with other codes and theories in Section IV. In Section V, we calculate the linear properties of the EP excited TAE using DAEPS. In the last section, we give a brief summary of the current DAEPS development status and discuss the future work.

II. DAEPS Model Equations

The model equations for the Drift Alfvén Energetic Particle Stability code (DAEPS code) are originated from the general fishbone-like dispersion relation (GFLDR) [29, 30]. The theoretical framework of GFLDR can be used to analyze SAW/DAW physics by adopting the mode structure decomposition (MSD) method [31] and asymptotic matching between the inertial region/singular layer and the ideal region [15]. The GFLDR, for a single n toroidal mode, takes the form of $i|s|\Lambda_n = \delta\hat{W}_{nf} + \delta\hat{W}_{nk}$, where

the generalized inertial term Λ_n is the normalized singular layer contribution including kinetic response, s is the magnetic shear, $\delta\hat{W}_{nf}$ and $\delta\hat{W}_{nk}$ are the fluid and kinetic contributions of the potential energy, respectively. The dispersion relation can be formulated in a quadratic form due to the variational nature of GFLDR. A trial function is needed to calculate the frequency, growth rate, fluid and kinetic potential energies and their asymptotic behaviors, which needs to be accurate enough in the asymptotic limit for a precise calculation of the linear eigenvalues. For high toroidal mode number n, when radial envelope variation can be ignored in the lowest order, GFLDR becomes the local dispersion relation $i\Lambda_n = \delta\bar{W}_{nf} + \delta\bar{W}_{nk}$, where $\delta\bar{W}_n = \delta\hat{W}_n / |s|$ for localized modes.

The mode structure decomposition [31] is valid for general toroidal mode number n, which introduces the projection operator transforming the fluctuation function f from real space $f(r,\theta,\zeta)$ to the mode structure decomposition (MSD) space $\hat{f}_n(r,\vartheta)$, i.e., $\mathcal{P}_{Bn} : f(r,\theta,\zeta) \mapsto \hat{f}_n(r,\theta)$, which takes the form of :

$$f(r,\theta,\zeta) = \sum_m e^{in\zeta - im\theta} \int e^{i(m-nq)\vartheta} \mathcal{P}_{Bn}(r,\vartheta)[f]\, d\vartheta \quad , \tag{1}$$

where $\mathcal{P}_{Bn}$ is the function mapping between the two spaces. For high n mode with moderate to high magnetic shear, the unstable modes are localized around the mode rational surface, the envelope variation is weak, and the MSD can be reduced to the ballooning representation [31]:

$$f(r,\theta,\zeta) = \sum_{n,m} A_n(r) e^{in\zeta - im\theta} \int e^{i(m-nq)\vartheta} \mathcal{P}_{Bn}(r,\vartheta)[f_{0n}]\, d\vartheta \quad , \tag{2}$$

where the fluctuation function f shows a two-scale feature in the radial structure with f_{0n} varying in the micro-scale $\Delta_0 = (nq')^{-1}$ and macro-scale $O(a)$, and the envelope function $A_n(r)$ varying in the meso-scale $(\Delta_0 a)^{1/2}$ which can be further described by an eikonal ansatz $A_n(r) \sim \exp\left[i \int nq' \vartheta_k(r)\, dr \right]$.

The DAEPS model equations assume the gyrokinetic ordering and solve the gyrokinetic-Maxwell system by singling out essential kinetic physics. The tearing mode physics is ignored, so the perturbed parallel vector potential $\delta A_\parallel$ can be described by a magnetic scalar potential $\delta\psi$ with $\partial_t \delta A_\parallel = -c\partial_\parallel \delta\psi$. Using the s-α equilibrium model, the following vorticity equation is solved in the DAEPS model [32]:

$$B\partial_\parallel\left[\frac{1}{B}\frac{k_\perp^2}{k_\theta^2}\partial_\parallel\right]\delta\psi + \frac{\omega\left(\omega-\omega_{*pi}\right)}{v_A^2}\frac{k_\perp^2}{k_\theta^2}\delta\phi + \frac{\alpha}{q^2R^2}g\delta\psi = \sum_j\left\langle\frac{4\pi q_j}{k_\theta^2 c^2}J_0\omega\omega_{dj}\delta K_j\right\rangle_v, \quad (3)$$

where the left hand side (LHS) is the fluid contribution, consisting of field line bending, inertial and ballooning interchange, and the right hand side (RHS) is the kinetic compression, which could come from either energetic particles or thermal particle. $\alpha = -Rq^2\beta'$ with $\beta = 8\pi P/B^2$ is the dimensionless pressure gradient that provides instability drive, $k_\theta = \frac{nq}{r}$, $\omega_{*pi} = \frac{\mathbf{k}\times\mathbf{b}}{\Omega_{ci}m_i}\cdot\nabla P_i$ is the ion diamagnetic frequency, $\omega_{dj} = \mathbf{b}\times\left(\mu\nabla B + v_\parallel^2\boldsymbol{\kappa}\right)/\Omega_{cj}$ is the drift frequency for the particle species j, q is the safety factor, the q_j is the charge for the particle species j, and $\langle\cdots\rangle_v = \int(\cdots)d^3\mathbf{v}$ denotes integration over the velocity space, $v_A = \frac{B}{\sqrt{4\pi nm}}$ is the Alfvén velocity, $J_0 = J_0\left(k_\perp\rho_j\right)$ is the Bessel function of the first kind of zeroth order, $\rho_j = v_\perp/\Omega_{cj}$ is the Larmor radius with Ω_{cj} the cyclotron frequency, $k_\perp^2 = k_\theta^2\kappa_\perp^2$ with $\kappa_\perp^2 = 1+\left(s\theta-\alpha\sin\theta\right)^2$ and $g = \cos\theta - \left(s\theta-\alpha\sin\theta\right)\sin\theta$, $\partial_\parallel = \frac{\mathbf{B}}{B}\cdot\nabla = \frac{1}{qR}\partial_\theta$, and θ is the extended poloidal angle in the cover space of the ballooning representation.

The fluid contribution of energetic particles is assumed negligible. The ideal MHD approximation $\delta E_\parallel = \partial_\parallel\delta\phi - c^{-1}\partial_t\delta A_\parallel = 0$ is used for convenience to give $\delta\phi = \delta\psi$, which is valid for linear physics of BAE and EP excited TAE [9, 32], and thus the quasi-neutrality condition is no longer necessary. For most relevant cases we consider high n modes, thus in the ballooning representation the vorticity equation of Eq. (3) can be

written explicitly as [32, 34]:

$$\partial_\theta k_\perp^2 \partial_\theta \delta\psi + \frac{\omega\left(\omega-\omega_{*pi}\right)}{\omega_A^2} k_\perp^2 \delta\psi + \alpha g \delta\psi = \sum_j \left\langle \frac{4\pi q_j q^2 R^2}{c^2} J_0\left(k_\perp \rho_j\right) \omega \omega_{dj} \delta K_j \right\rangle_v . \quad (4)$$

In Eq. (4), ω_A is the Alfvén frequency with $\omega_A^2 = \left(\frac{v_A}{qR}\right)^2 = \omega_{A0}^2\left(1-4\epsilon\cos\theta\right)$ for a large aspect ratio with circular flux surface tokamak with $\epsilon = r/R$, where ω_{A0} is the Alfvén frequency on the magnetic axis that determines the basic characteristic time scale for Eq. (4).

The gyrocenter distribution function δK_j can be solved through the linearized collisionless electromagnetic gyrokinetic equation:

$$\left(\frac{v_\parallel}{qR}\partial_\theta - i\omega + i\omega_{dj}\right)\delta K_j = i\frac{q_j}{m_j} Q F_{0j} \frac{\omega_{dj}}{\omega} J_0\left(k_\perp \rho_j\right)\delta\psi \quad , \quad (5)$$

where $QF_{0j} = \left(\omega\partial_E + \hat{\omega}_{*j}\right)F_{0j}$ is the free energy provided by the phase space gradient of the equilibrium distribution function F_{0j}, with $E = \frac{1}{2}v^2$ and $\hat{\omega}_{*j} = \Omega_{cj}^{-1}\mathbf{k}\times\mathbf{b}\cdot\nabla$.

The asymptotic behavior of $\delta\psi$ as $\theta \to \pm\infty$, which is critical for calculating the eigen frequency and growth rate and identifying whether a mode is physical or spurious, is determined by the outgoing wave boundary condition with causality constraints. In order to properly handle the asymptotic behavior, the vorticity equation should be written as the Schrödinger-like form:

$$\left[\partial_\theta^2 + \frac{\omega\left(\omega-\omega_{*pi}\right)}{\omega_A^2} + V\left(\theta\right)\right]\Psi = \sum_j \left\langle \frac{4\pi q_j q^2 R^2}{k_\theta^2 c^2 \kappa_\perp} J_0 \omega \omega_{dj} \delta K_j \right\rangle_v \quad , \quad (6)$$

where $V\left(\theta\right) = \kappa_\perp^{-2}\alpha\cos\theta - \kappa_\perp^{-4}\left(s-\alpha\cos\theta\right)^2$ is the effective potential well, and $\Psi = \kappa_\perp \delta\psi$ is the perturbed magnetic scalar potential, whose asymptotic behavior can be derived by taking the limit $\theta \to \pm\infty$. Ignoring the variation of magnetic field along the field line, the asymptotic behavior will be described by a wave equation:

$$\left(\partial_\theta^2 + \Lambda^2\right)\Psi = 0 . \quad (7)$$

Employing the outgoing wave boundary condition, the asymptotic behavior of the

perturbed magnetic scalar potential takes the form of:

$$\lim_{\theta\to\pm\infty}\Psi = e^{i\Lambda|\theta|}\ , \tag{8}$$

where Λ is the inertial term in the GFLDR [15, 29, 30], which contains the kinetic contribution. The continuous spectrum corresponds to purely real Λ, while the discrete spectrum corresponds to purely imaginary Λ [32].

Considering the periodic variation in ω_A along the field line due to the periodicity of magnetic field, the asymptotic behavior of Ψ can be expressed in the following form using the Floquet theory [30, 35]:

$$\lim_{\theta\to\pm\infty}\Psi = e^{i\nu|\theta|}P(\theta), \tag{9}$$

where $P(\theta)$ is a 2π-periodic function. The causality constraint requires $\mathrm{Re}\,\nu > 0$ for the outgoing wave boundary condition.

The RHS of Eq. (6) involves the integration of perturbed gyrocenter distribution function δK_j, which can be solved from Eq. (5). Considering only the circulating particle response, the gyrokinetic equation can be integrated directly in the ballooning space [26-28] as:

$$\begin{aligned}\delta K_j(\theta,\hat{\sigma},\lambda,E) &= \int_{\theta}^{-\hat{\sigma}\,\infty}\exp\left[i\,\mathrm{sign}(\mathrm{Im}\,\omega)\int_{\theta}^{x}qR\frac{-\omega+\omega_{dj}(y)}{|v_{\|}|}dy\right]\\ &\times\ (-\hat{\sigma})i\frac{q_j}{m_j}\frac{qR}{|v_{\|}|}QF_{0j}\frac{\omega_{dj}(x)}{\omega}J_0\frac{\Psi(x)}{\kappa_{\perp}(x)}dx\end{aligned}\ , \tag{10}$$

where $\hat{\sigma}=\dfrac{v_{\|}}{|v_{\|}|}$ is the direction of parallel velocity, $\lambda=\dfrac{\mu B_0}{E}$ is the velocity pitch angle, and the signum function of the imaginary part of ω is the causality constraint to avoid the integral divergence. Hence, the kinetic compression term (KC) can be written as:

$$
\begin{aligned}
\mathrm{KC} &= \kappa_{\perp}^{-1}\left\langle \frac{4\pi q_j q^2 R^2}{k_\theta^2 c^2}\omega\omega_{dj} J_0 \delta K_j \right\rangle_v \\
&= \frac{4\pi q_j q^2 R^2}{k_\theta^2 c^2}\int_0^\infty dE\int_0^1 d\lambda\int_{-\infty}^{\infty} dx \frac{2\pi E}{|v_\parallel|}\frac{\omega_{dj}(\theta)}{\kappa_\perp(\theta)} J_0 i \frac{q_j}{m_j}\frac{qR}{|v_\parallel|} Q F_{0j} \quad . \qquad (11) \\
&\times \exp\left[i\,\mathrm{sign}\left(\mathrm{Im}\,\omega(\theta-x)\right)\int_\theta^x dy \frac{-\omega+\omega_{dj}}{|v_\parallel|} qR \right]\frac{\omega_{dj}(x)}{\kappa_\perp(x)} J_0 \Psi(x)
\end{aligned}
$$

Thus, the DAEPS model equation becomes an integral-differential equation that manifests itself a nonlinear eigenvalue problem. Appropriate numerical method needs to be found to solve this equation, as shown in the next section.

III. Numerical Method

The DAEPS code uses the finite element method with cubic B-Spline to solve Eq. (6) with special elements near boundaries [36]. For total N grid points in the extended poloidal angle domain with equal grid step h, the finite element basis function $|n\rangle, (2 \le n \le N-2)$, lies in region $(n-2)h < x < (n+2)h$, and takes the form of:

$$
|n\rangle = \phi\left(\frac{x}{h} - n\right) \quad , \qquad (12)
$$

where $\phi(x)$ is a piecewise function:

$$
\phi(x) = \begin{cases}
\frac{4}{3} + 2x + x^2 + \frac{x^3}{6} & -2 \le x < -1 \\
\frac{2}{3} - x^2 - \frac{x^3}{2} & -1 \le x < 0 \\
\frac{2}{3} - x^2 + \frac{x^3}{2} & 0 \le x < 1 \\
\frac{4}{3} - 2x + x^2 - \frac{x^3}{6} & 1 \le x \le 2
\end{cases} \quad . \qquad (13)
$$

For the special elements near the left boundary $x = x_L$, the boundary elements $|-1\rangle$, $|0\rangle$ and $|1\rangle$ take the form of:

$$
\begin{aligned}
|-1\rangle(hy+x_L) &= 1-3y+3y^2-y^3 \qquad 0\le y\le 1 \\
|0\rangle(hy+x_L) &= \begin{cases} y-\frac{3}{2}y^2+\frac{7}{12}y^3 & 0\le y<1 \\ \frac{2}{3}-y+\frac{1}{2}y^2-\frac{1}{12}y^3 & 1\le y\le 2 \end{cases} \\
|1\rangle(hy+x_L) &= \begin{cases} \frac{1}{2}y^2-\frac{11}{36}y^3 & 0\le y<1 \\ -\frac{1}{2}+\frac{3}{2}y-y^2+\frac{7}{36}y^3 & 1\le y<2 \\ \frac{3}{2}-\frac{3}{2}y+\frac{1}{2}y^2-\frac{1}{18}y^3 & 2\le y\le 3 \end{cases}
\end{aligned}
\qquad (14)
$$

As shown in the Fig. 1, these special elements near the boundaries have their special properties, where $|-1\rangle$ has non-zero value at the boundary, while $|-1\rangle$ and $|0\rangle$ have non-zero derivatives at the left boundary. These properties particularly favor Dirichlet and Neumann boundary condition.

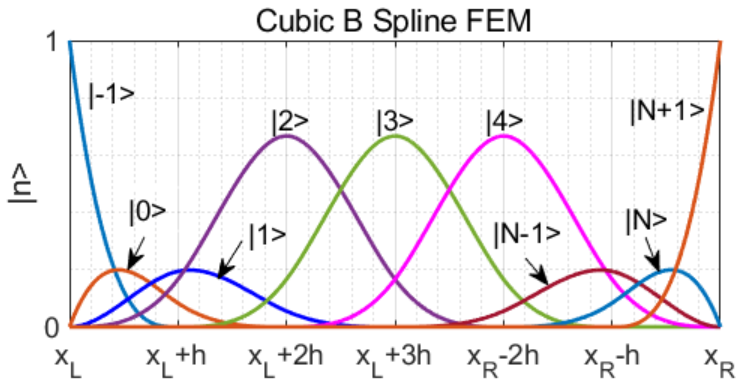

Figure 1: The B-Spline finite element with $N=6$ grid within the interval $[x_L, x_R]$.

The perturbed magnetic scalar potential in Eq. (6) can be expressed by a linear combination of the finite elements $|n\rangle$, i.e., $\Psi(\theta)=\sum_{n=-1}^{N+1} a_n|n\rangle(\theta)$. Hence, the weak form of Eq. (6) takes the form of:

$$
\begin{aligned}
\sum_{n=-1}^{N+1} a_n \langle m|\mathrm{KC}|n\rangle \;=\; & \sum_{n=-1}^{N+1} a_n \Big[-\left(\partial_\theta|m\rangle\right)^\dagger \partial_\theta|n\rangle + \langle m|\partial_\theta|n\rangle_{\theta_-}^{\theta_+} \\
& + \langle m|\frac{\omega(\omega-\omega_{*pi})}{\omega_A^2}+V(\theta)|n\rangle \Big]
\end{aligned}
\qquad (15)
$$

where the computational domain is taken as $[\theta_-, \theta_+]$, and the boundary condition term

$\langle m|\partial_\theta|n\rangle$, considering the Neumann boundary condition $\partial_\theta\Psi|_{\theta\to\theta_\pm}=\pm i\Lambda\Psi$, can be transformed to:

$$\langle m|\partial_\theta|n\rangle_{\theta_-}^{\theta_+}=i\Lambda\left[\langle m|n\rangle(\theta_+)+\langle m|n\rangle(\theta_-)\right]. \tag{16}$$

Such a boundary condition is essentially an absorbing boundary condition for outgoing wave with no reflection for given asymptotic behavior, which is important for the causality constraint. The self-adjointness of the LHS of Eq. (6) requires that the eigenfunctions appear in complex conjugate pairs in the ideal MHD limit, where the eigenmode structure Ψ and its complex conjugate Ψ^* are both eigenfunctions with the same eigenvalue, and with opposite signs for the real part of the asymptotic parameter Λ, which denote two opposite propagation directions for the wave. The causality constraint $\mathrm{Re}\Lambda>0$ suggests that there should exist only one physical solution in each pair of solutions [29]. However, with improper boundary condition that reflects the outgoing wave backwards, the calculated mode structure Ψ is superimposed by the unphysical reflected mode Ψ^*, which leads to the inaccuracy in the eigenfunction and the corresponding eigenvalue.

The FEM weak form of Eq. (6), as shown in Eq. (15), is closely related to the GFLDR framework [29, 30]. By multiplying the complex conjugate of FEM coefficient $a_n^\dagger$ and performing the summation over the FEM space, the left hand side (LHS) of Eq. (15) is the local kinetic contribution to the potential energy $\delta\bar{W}_k$. The non-boundary terms in the right hand side (RHS) are the local fluid contribution to the potential energy $\delta\bar{W}_f$, and the boundary term is the inertial term in GFLDR. Since the computational domain should include the ideal region $\theta\ll 1$, the boundary condition Eq. (16) at computational boundary $\theta_\pm$ is essentially performing the asymptotic matching for Ψ from the ideal region to the inertial region, i.e., $\Psi_{ID}^\dagger\partial_\theta\Psi_{ID}|_{-\infty}^{+\infty}=\Psi_{IN}^\dagger\partial_\theta\Psi_{IN}|_{-0}^{+0}=2i\Lambda$, which suggests that the computational domain should be large enough to cover the inertial region. Using the DAEPS model, both fluid and kinetic contributions to the potential energy and singular layer can be accurately calculated, and the solution to the

FEM weak form of DAEPS equation can automatically satisfy the GFLDR equation. Using the FEM, the matrix form of the vorticity equation Eq. (15) becomes a nonlinear eigenvalue equation: $\vec{\vec{A}}(\Lambda,\omega)\mathbf{x}+\omega\vec{\vec{B}}\mathbf{x}+\vec{\vec{C}}\mathbf{x}=0$. Here an iterative algorithm is designed to solve the eigen frequency ω and the asymptotic behavior of the mode structure Λ, where ω is calculated from the eigenvalue of the matrix, the asymptotic behavior is fitted from the eigenvector of the matrix, and both of them are reserved for next iteration until the convergence is achieved.

We note that the kinetic compression term KC, on the LHS of Eq. (15), involves a multidimensional integration:

$$\begin{aligned}\sum_{n=-1}^{N+1} a_n \langle m|\mathrm{KC}|n\rangle &= \frac{4\pi q_j q^2 R^2}{k_\theta^2 c^2}\sum_{n=-1}^{N+1}\int_{-\infty}^{\infty}d\theta\int_0^{\infty}dE\int_0^1 d\lambda\int_{-\infty}^{\infty}dx\frac{2\pi E}{|v_\parallel|}\frac{\omega_{dj}(\theta)}{\kappa_\perp(\theta)}J_0 \\ &\times i\frac{q_j}{m_j}\frac{qR}{|v_\parallel|}QF_{0j}\langle m|(\theta)\frac{\omega_{dj}(x)}{\kappa_\perp(x)}J_0 a_n|n\rangle(x) \\ &\times \exp\left[i\,\mathrm{sign}\left(\mathrm{Im}\,\omega(\theta-x)\right)\int_\theta^x dy\frac{-\omega+\omega_{dj}}{|v_\parallel|}qR\right]\end{aligned} \quad , (17)$$

where we use the numerical method of global h-adaptive multidimensional integration over hypercube [37, 38] to calculate the KC term, and piecewise Gauss-Legendre quadrature to calculate the FEM integral.

IV. BAE/KBM with Kinetic Thermal Ions

Beta-induced Alfvén eigenmode (BAE) exists in the finite pressure induced gap for the Alfvén continuum, which is caused by the coupling between SAW and sound wave (SW) induced by plasma compressibility [8, 12]. BAE can be excited by the plasma compressibility from either thermal ions or energetic particles via wave-particle resonance [32].

For simplicity, here we only consider the BAE excited by the circulating thermal particles. Since the BAE is a $k_\parallel \approx 0$ mode, the mode structure of BAE in the ballooning representation varies slowly with the extended poloidal angle θ in the inertial region, which means the real part of asymptotic behavior $\mathrm{Re}\,\Lambda$ is small [6].

Hence BAE is a long wavelength mode, $\Lambda \sim q\sqrt{\beta}$, the ideal MHD assumption of neglecting parallel electric field holds, $\delta E_{\parallel} \approx 0$, [6], since BAE propagates in the ion diamagnetic direction [32]. The KC term in Eq. (17) can be simplified using the drift center transformation. By expanding the pull-back operator $\exp\left(-ik_{\perp}\rho_{dj}\cos\theta\right)$ to the lowest order [10, 34] and performing scale separation between the fast variation $\theta_0 \sim O(1)$ and slow variation $\theta_1 \gg 1$, the reduced kinetic compression term takes the form of:

$$\mathrm{KC} \approx \frac{4\pi q_j q^2 R^2}{k_\theta^2 c^2}\left\langle \frac{q_j}{m_j} QF_{0j}\omega_{tj}^2 J_0^2 J_1^2 \frac{4\omega\left(1-\cos 2\theta\right)}{\omega_{tj}^2-\omega^2}\frac{\Psi}{\kappa_\perp^2}\right\rangle_v , \tag{18}$$

where $\omega_{tj} = \dfrac{|v_{\parallel}|}{qR}$ is the transit frequency, $J_1 = J_1\left(k_\perp \rho_{dj}\right)$ is the Bessel function of the first kind of first order, and $\rho_{dj} = \dfrac{\Omega_{dj}}{k_\theta \omega_{tj}}$ is the drift-orbit width with $\Omega_{dj} = \omega_{dj}/g$. The term $\left(\omega_{tj}^2 - \omega^2\right)^{-1}$ is identified as the transit resonant interaction between particle and wave. Ignoring the FOW and FLR effects, the kinetic compression term in Eq. (11) can also be further simplified by assuming the aforementioned scale separation:

$$\mathrm{KC} = \frac{4\pi q_j q^2 R^2}{k_\theta^2 c^2}\left\langle \frac{q_j}{m_j} QF_{0j}\Omega_{dj}^2 \sin^2\theta \frac{\omega}{\omega_{tj}^2-\omega^2}\Psi\right\rangle_v . \tag{19}$$

It is known that the BAE branch can be coupled with kinetic ballooning mode (KBM) branch in some parameter regime [32]. Here for the code benchmark purpose, we first choose the KBM instability, which is also a small $k_{\parallel}$ mode, excited by only thermal ions. Fig. 2(a) shows the comparison of the real frequency and growth rate between DAEPS and the initial value linear gyrokinetic PIC code AWECS [25], with the prescribed plasma parameters $q = 1.2$, magnetic shear $s = 0.4$, $\epsilon_{ni} = L_{ni}/R = 0.175$, with $L_{ni} = -\partial_r \ln n_i$, $\eta_i = \dfrac{d\ln T_i}{d\ln n_i} = 2$. In Fig 2(a), the solid line and dashed line show the eigen frequency and growth rate vs. the dimensionless pressure gradient α

respectively, the blue squares are from DAEPS with reduced KC, the red triangles are from DAEPS with complete KC, and the black circles are from the AWECS result. The DAEPS result is fully consistent with the AWECS result. In addition, we note that the difference in the linear frequency, growth rate and asymptotic behavior is less than 10% between the reduced KC and complete KC, as shown by Fig. 2(a) & (b). The small differences between DAEPS and AWECS can be attributed to the ion polarization and parallel electric field ignored in the DAEPS model for simplicity. The comparison of the KBM eigenvalue and asymptotic behavior suggests that using the reduced form of KC in the DAEPS code can accelerate the calculation of the eigenvalue and asymptotic behavior without losing accuracy to a speed dozens of times faster than using the complete KC term by substantially reducing numerical integration time.

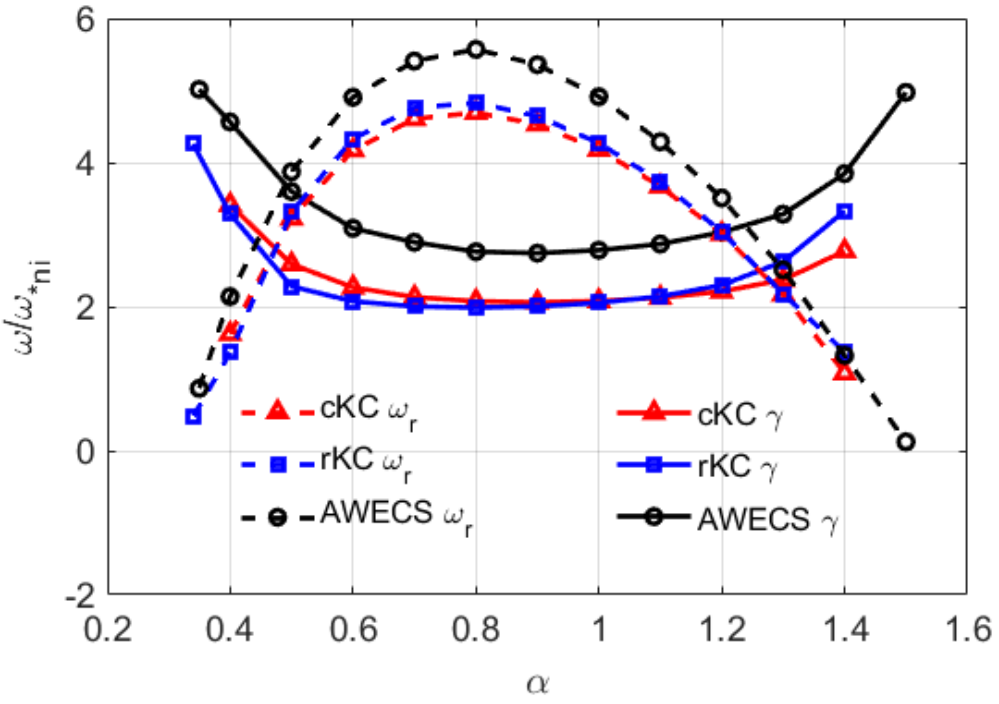

(a)

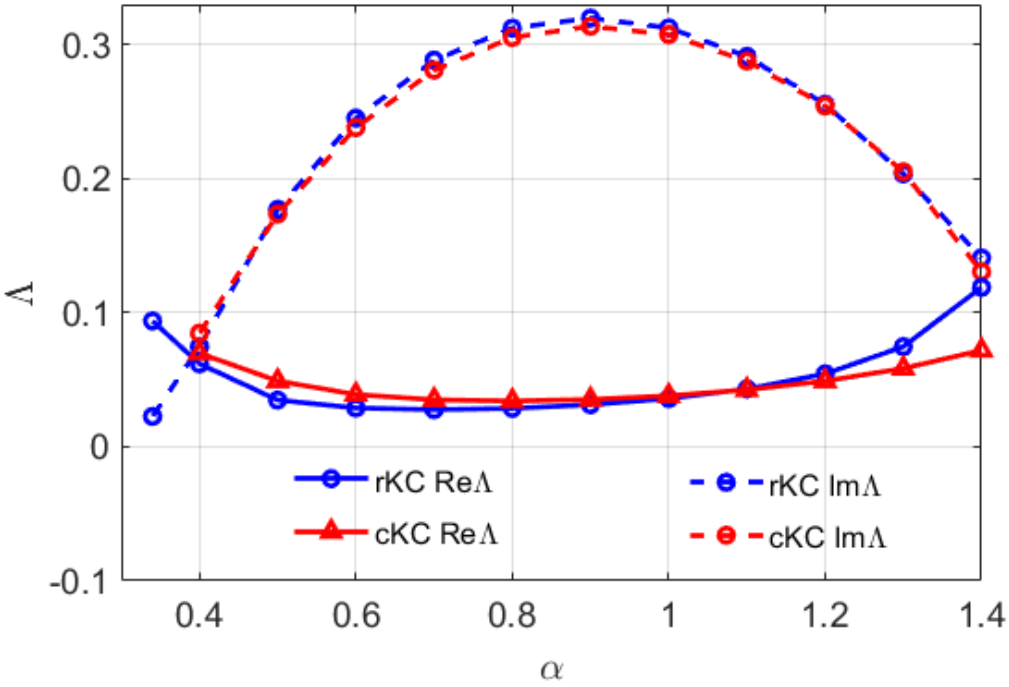

(b)

Figure 2: Comparison of linear dispersion and eigenmode asymptotic behavior for KBM between the DAEPS results with complete KC term (cKC) and reduced KC term (rKC).(a) real frequency ω_r and growth rate γ vs α; (b) asymptotic behavior Λ vs α.

Next we show the benchmark for the BAE instability. According to the GFLDR theory, the BAE dispersion relation, after assuming $\omega \sim \omega_{ti} \sim \omega_{*pi} \ll \omega_A$, is given by the following equation [32]:

$$\left\{\frac{\omega\left(\omega-\omega_{*pi}\right)}{\omega_A^2}+q^2\frac{\omega_{ti}}{\omega_A^2}\left[\left(\omega-\omega_{*ni}\right)F\left(\frac{\omega}{\omega_{Ti}}\right)-\omega_{*Ti}G\left(\frac{\omega}{\omega_{Ti}}\right)-\frac{N^2\left(\omega/\omega_{Ti}\right)}{D\left(\omega/\omega_{Ti}\right)}\right]\right\}^{1/2}=\Lambda, \quad (20)$$

where $\omega_{Ti}=\sqrt{\frac{2T_i}{m_i}}\frac{1}{qR}$, and the functions, $F(x)$, $G(x)$, $N(x)$ and $D(x)$ are introduced by Ref. [32]:

$$N(x)=\left(1-\frac{\omega_{*ni}}{\omega}\right)\left[x+\left(\frac{1}{2}+x^2\right)Z(x)\right]-\frac{\omega_{*Ti}}{\omega}\left[x\left(\frac{1}{2}+x^2\right)+\left(\frac{1}{4}+x^4\right)Z(x)\right]$$
$$D(x)=\frac{1}{x}\left(1+\frac{1}{\tau}\right)+\left(1-\frac{\omega_{*ni}}{\omega}\right)Z(x)-\frac{\omega_{*Ti}}{\omega}\left[x\left(\frac{1}{2}+x^2\right)+\left(\frac{1}{4}+x^4\right)Z(x)\right]$$
$$F(x)=x\left(x^2+\frac{3}{2}\right)+\left(x^4+x^2+\frac{1}{2}\right)Z(x)$$
$$G(x)=x\left(x^4+x^2+2\right)+\left(x^6+\frac{x^4}{2}+x^2+\frac{3}{4}\right)Z(x) \quad . \quad (21)$$

According to the theory, there exists a critical value for η_i, below which the KBM branch is the most unstable branch, and above which the coupled BAE and KBM branch is the most unstable branch. In order to better estimate the value of Λ in the theory, the asymptotic behavior value Λ calculated by the DAEPS code is substituted back into the Eq. (20) to compute the linear frequency and growth rate. An example is shown in Fig. 3 with the plasma parameters $\beta_i=0.01$, $q=1.5$, $\omega_{*ni}=\omega_{ti}$, and $\eta_i>0.5$ is above the critical value, which ensures that the mode calculated by DAEPS stays in the coupled BAE/KBM branch, where the red triangles and diamonds are from the DAEPS code with complete KC term (cKC) and reduced KC term (rKC) respectively, and the blue circles and squares are from theory given by Eq. (20) with complete KC term (cKC) and reduced KC term (rKC) respectively. As shown in Fig. 3(a), the increasing trend of eigen frequency and growth rate with increasing η_i calculated by the DAEPS code is qualitatively consistent with the theory for both complete KC and reduced KC case. The notable shift between DAEPS and theory in Fig. 3(a) is presumably caused by the FOW and FLR effects, which are treated as higher order and neglected in the conventional theory [32]. To verify this conjecture, we compare the DAEPS results using the reduced KC ignoring the FLR and FOW effects in Eq. (19) with the conventional theory in Eq. (20) on the BAE/KBM instability. As shown in Fig. 3(b), the difference in the eigen frequency, growth rate and asymptotic behavior is negligibly small between DAEPS and theory, and the discrepancy is actually less than 10% between DAEPS result using reduced KC term and using complete KC term, which proves that the large discrepancy between DAEPS and theory in Fig. 3(a) is due to the

FOW and FLR effects and also verifies the validity of using the reduced KC term in the DAEPS code to accelerate computation. The comparisons in Figs. 3(a) & (b) also demonstrate the stabilizing nature of the FLR and FOW effects in the BAE excitation. The conventional theory overestimates the BAE instability threshold and gives a much larger linear grow rate close to marginal stability, which would affect the nonlinear physics profoundly, especially comparing to experiments.

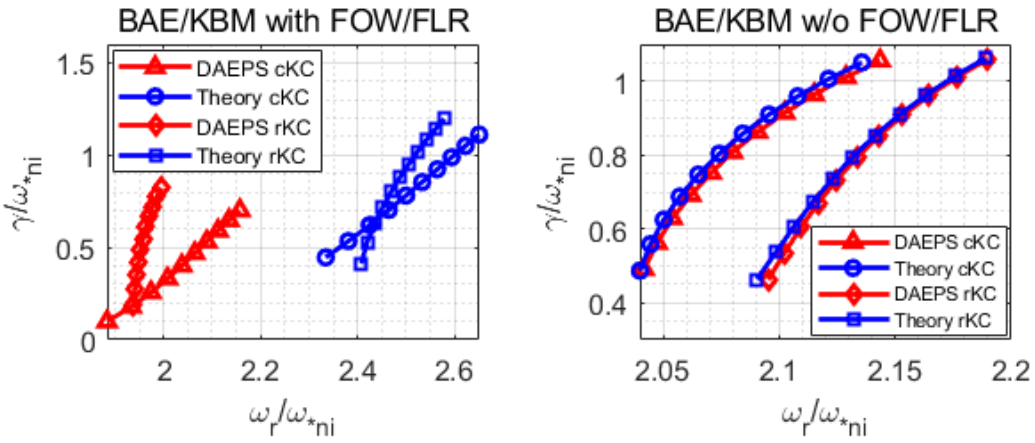

(a) (b)

Figure 3: Comparison of real frequency ω_r and growth rate γ from the DAEPS code and theory for various η_i: (a) eigenvalue comparison with FLR and FOW effects; (b) eigenvalue comparison without FLR and FOW effects.

The asymptotic behavior is crucial to solve the eigen frequency and growth rate when the mode structure in the inertial region is more important than in the ideal region, which often occurs for the marginally unstable or damping modes, as well as for the continuous spectrum located only in the inertial region, such as the Alfvén continuous spectrum to be introduced in the next section. Since BAE/KBM mode is strongly MHD unstable, the asymptotic behavior is not crucial for calculating the eigen frequency and growth rate of BAE/KBM. However, the computation cost is substantially reduced with the proper boundary condition since much narrower computational domain is needed, as is demonstrated by following. Here we use the BAE/KBM typical parameters with

$\eta_i = 0.7$ in the preceding study to perform a comparison between the cases with and without the proper boundary condition for the correct asymptotic behavior, where the case without the proper boundary condition is calculated by using the free boundary condition $\partial_\theta \Psi = 0$. Fig. 4(a) shows the comparison of the mode structures with different boundary conditions, where the red solid line and the blue dashed line are the real and imaginary parts of the mode structure with the proper BC, while the red circles and blue diamonds are the real and imaginary parts of the mode structure without the proper BC. As is shown in the Fig. 4(a), the difference between these two different BC cases becomes significant in the inertial region, where the logarithm of the mode structure should be described by the linear relationship $\log \Psi = i\Lambda|\theta| + \text{const}$ as is required by the correct asymptotic behavior. A large discrepancy occurs in the inertial region for the logarithm of the mode structure without the proper BC when fitting with the linear relation, as shown in Figs. 4(b) & (c), where the black dotted line is the linear fitting of the logarithm of the mode structure with the proper BC; the red solid line and red circles are the real part of the logarithm of mode structure with and without the proper BC, respectively; and blue dashed line and blue diamonds are the imaginary part of the logarithm of mode structure with and without the proper BC, respectively.

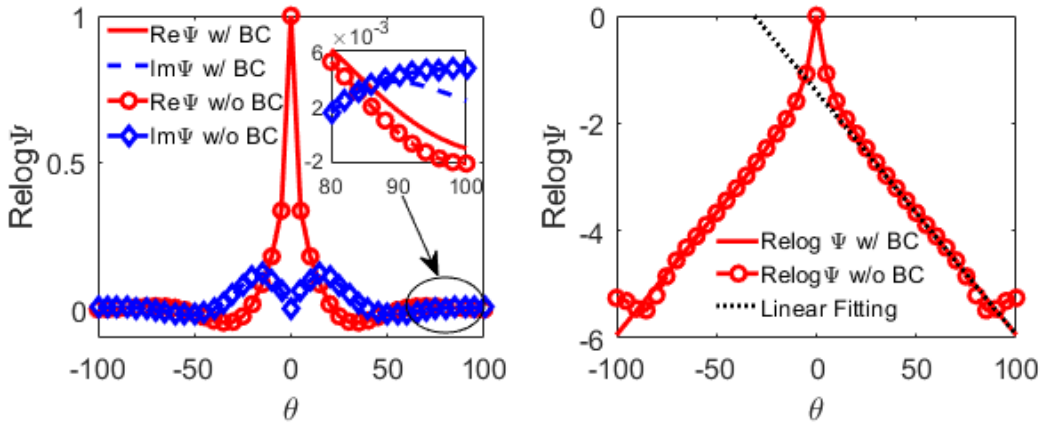

(a) (b)

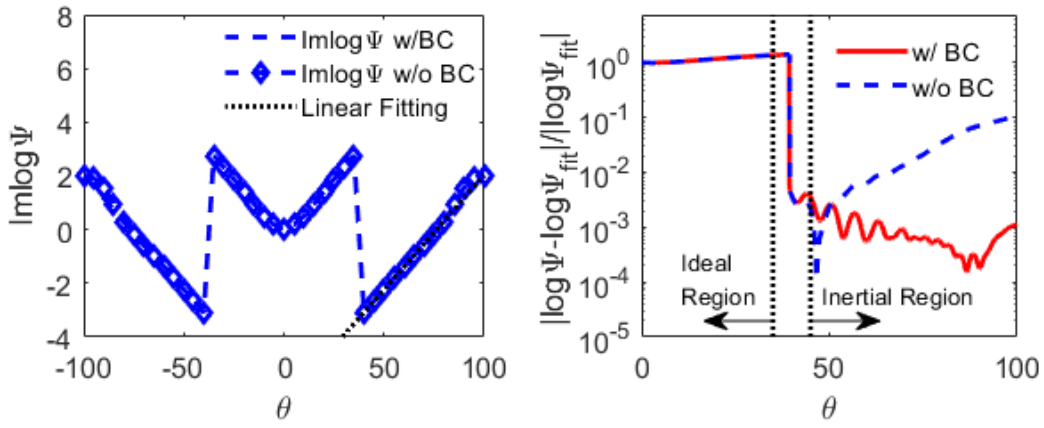

(c) (d)

Figure 4: Comparison of the mode structures with $\eta_i = 0.7$ for the DAEPS results with (w/) and without (w/o) the proper boundary condition (BC): (a) mode structure for real and imaginary parts of Ψ in linear scale; (b) real part of the logarithm of mode structure; (c) real part of the logarithm of mode structure, where the black dotted line is a linear fitting of the logarithm of the mode structure with the proper BC; (d) relative error of the asymptotic behavior in logarithmic scale.

The relative error of the asymptotic behavior is shown in Fig. 4(d) for the DAEPS results with and without the proper BC, denoted by the red solid line and the blue dashed line, respectively. The error of the asymptotic behavior at the boundary can propagate towards the ideal region, as shown in the Fig. 4(d), which could lead to a significant error in the calculated eigenvalue when the error propagated from the inertial region is large enough to affect the mode structure in the ideal region. Since the error of the asymptotic behavior decays exponentially as it propagates towards the ideal region, we can set the computational domain wide enough to eliminate the inaccuracy in the ideal region, which requires a fair amount of extra computing resources for the case without the proper BC.

In short, it is important to implement the correct asymptotic behavior for the following reasons: (1) the asymptotic behavior is crucial for calculating marginally unstable or damping modes when the mode structure in the inertial region is more important than that in the ideal region; (2) the computational domain needs only to cover a relatively small part of the inertial region to save computing resources; (3) the

solution to the DAEPS equation can automatically satisfy the GFLDR equation when including the correct asymptotic behavior, which can help us more easily identify the essential EP and Alfvénic physics.

V. Circulating Energetic Particle Excited TAE

The poloidal symmetry breaking of the equilibrium magnetic field, due to its non-uniformity in a flux surface, enables different poloidal harmonics to be coupled together, which can produce not only the frequency gaps in the SAW continuous spectrum but also discrete Alfvén eigenmodes which are localized in the forbidden band. The toroidicity-induced Alfvén eigenmode (TAE) is the discrete mode located inside the TAE gap. Since the coupling to the continuum can be ignored, the TAE is marginally stable and can be easily destabilized by EPs through wave-particle resonance [1, 39]. It is shown that TAE can cause resonant alpha particle loss even with low TAE amplitude [1, 14]. Therefore, the linear stability study of EP excited TAE is very important for the steady state operation of burning plasmas.

The SAW continuous spectrum is important because it determines the coupling of EP excited Alfvénic fluctuations to the continuous spectrum with continuum damping through phase mixing and mode structure localizations [39]. As is mentioned earlier, DAEPS can calculate marginally unstable and damping modes by incorporating the correct asymptotic behavior. As an application of this feature, we demonstrate here that the DAEPS code can also calculate the Alfvén continuous spectrum by ignoring the KC term and using the Floquet theory. Given toroidal and poloidal mode numbers (n,m), the frequency of the Alfvén continuum at flux surface r must satisfy $\nu^2(\omega,r)=\left[nq(r)-m\right]^2$. We have designed an algorithm to calculate the Floquet theory ν for the Alfvén continuum by linear fitting the logarithm of mode structure at the sample points $\log\Psi(2n\pi+\theta_0)$, where the computational domain should be inside the inertial region, $|\theta|\gg 1$. The Alfvén continuous spectrum calculated by DAEPS is compared with AWC [40], which is an ideal MHD global eigenvalue code, as shown in

Fig. 5(a) with concentric circular flux surfaces, inverse aspect ratio $\epsilon = \frac{a}{R} = 0.25$, toroidal mode number $n = 5$, and a parabolic q profile $q = 1 + \left(\frac{r}{a}\right)^2$, where a is the minor radius. The relative error between the DAEPS and AWC result is less than 0.1%. An example of the local dispersion curve of Alfvén continuous spectrum is shown in Fig. 5(b). After the calculation of the local dispersion curve on the each flux surface, the frequency of global Alfvén continuous spectrum of different toroidal and poloidal mode numbers on the given flux surface can be calculated using the frequency at given ν of the same local dispersion curve.

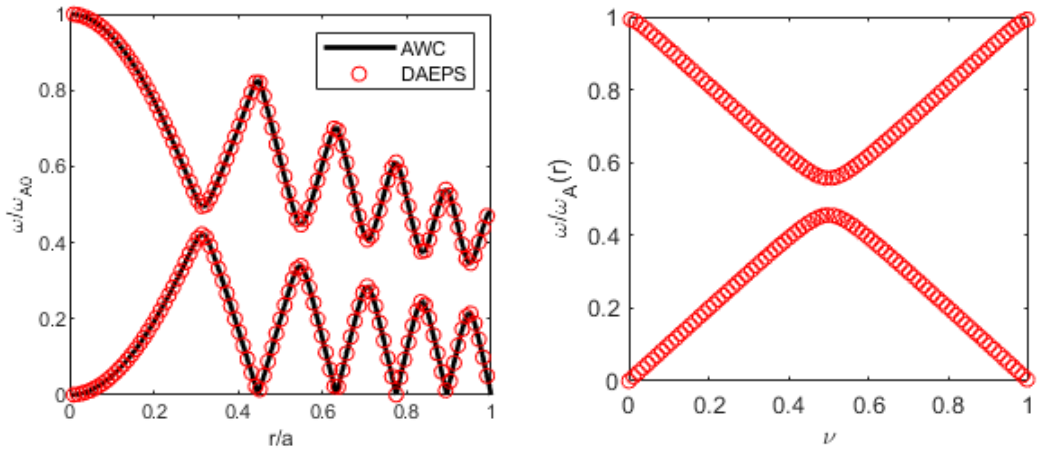

(a) (b)

Figure 5: Alfvén continuous spectrum calculated by DAEPS, where the solid lines are AWC result, red circles are DAEPS result. (a) Comparison of global Alfvén continuous spectrum with AWC result. (b) Local dispersion curve of Floquet theory ν at $r = 0.4a$ or $q = 1.16$ surface.

TAEs are marginally stable MHD modes, which can be easily excited by EPs, especially by circulating EPs. Therefore, the DAEPS code is first developed to calculate the TAE mode excited by the circulating energetic particles, assuming an ideal MHD background plasma and the KC term contributed by EP only. Fig. 6 shows the TAE numerical result by DAEPS with the prescribed plasma parameters $s = 0.2$, $q = 1.2$, $\epsilon = 0.15$, $\eta_E = 0.2$, $\epsilon_{nE} \equiv \frac{L_{nE}}{R_0} = 0.2$, $k_\theta \rho_E = 0.4$, $v_{tE} / v_A = 0.5$ and $\alpha = 0$ which

keeps the TAE frequency above the lower Alfvén continuum. For the benchmark purpose, the equilibrium energetic particle distribution is set as Maxwellian. As shown in Fig. 6(a), the TAE growth rate almost increases with the energetic particle pressure β_E linearly, which is consistent with the previous theory [9], where the ratio between the growth rate and frequency for circulating EP excited TAE is provided by [16]:

$$\frac{\gamma}{\omega} = \frac{4\pi^2 q^3 R}{B^2}\left\langle m_E\left(\frac{v_\perp^2}{2}+v_\parallel^2\right)^2 QF_{0E}\left[\delta\left(v_\parallel - v_A\right)+\frac{1}{3}\delta\left(v_\parallel-\frac{v_A}{3}\right)\right]\right\rangle_v , \qquad (22)$$

where δ is the Dirac delta function, which shows the resonant contribution from the $v_\parallel = v_A/3$ and $v_\parallel = v_A$ resonance, where the FLR and FOW effects are ignored in the theory. To compare DAEPS results with Eq. (22) in a more rigorous way, the FLR and FOW effects are ignored in the DAEPS equation. By substituting the frequency calculated by DAEPS into Eq. (22), we obtain the theoretical growth rate, which is then compared to the growth rate from DAEPS, as shown in Fig. 6(b). The relative difference in the growth rate between DAEPS and the theory is less than 1%. In addition, the growth rate without FLR and FOW effects in Fig. 6(b) is 6 times larger than the growth rate with FLR and FOW effects in Fig. 6(a), which suggests the stabilizing nature of the FLR and FOW effects in the TAE excitation. The poloidal mode coupling caused by FLR and FOW effect could have either stabilizing effect by suppressing the wave-particle resonance, or the destabilizing effect by involving more energetic particles in the wave-particle resonance [9]. In the parameter regime of this DAEPS calculation, the FLR and FOW effect is dominated by stabilization, because the stabilizing effect caused by the FLR and FOW due to the $v_\parallel = v_A/3$ resonance is more important than the destabilizing effect due to the $v_\parallel = v_A/5$ resonance as the EP distribution function is set as a local Maxwellian with EP thermal velocity $v_{tE} = v_A/2$ in this case.

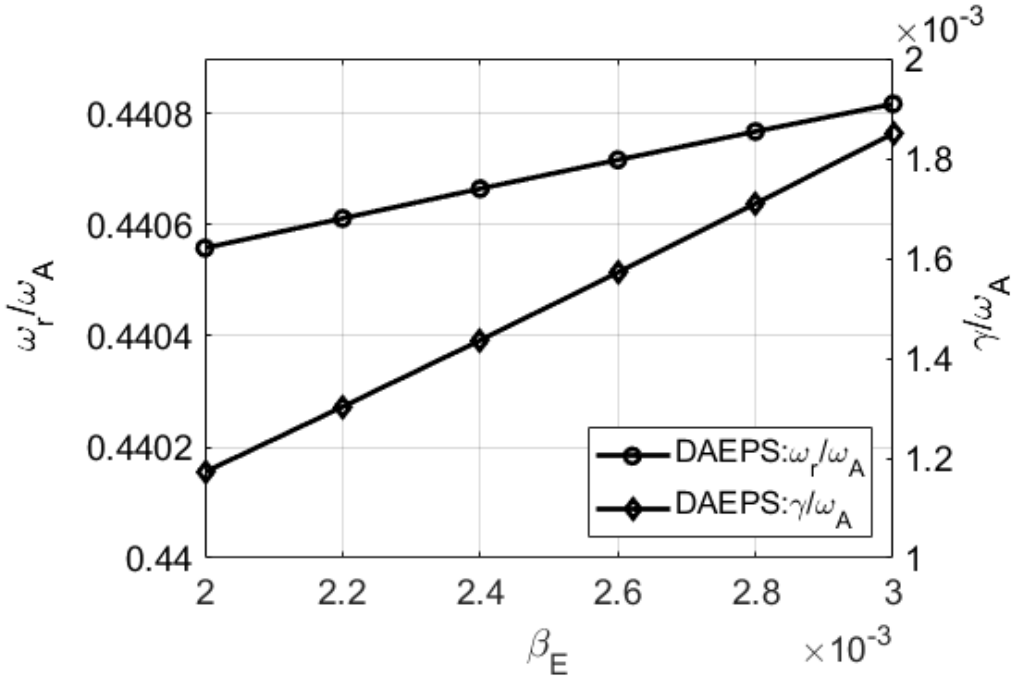

(a)

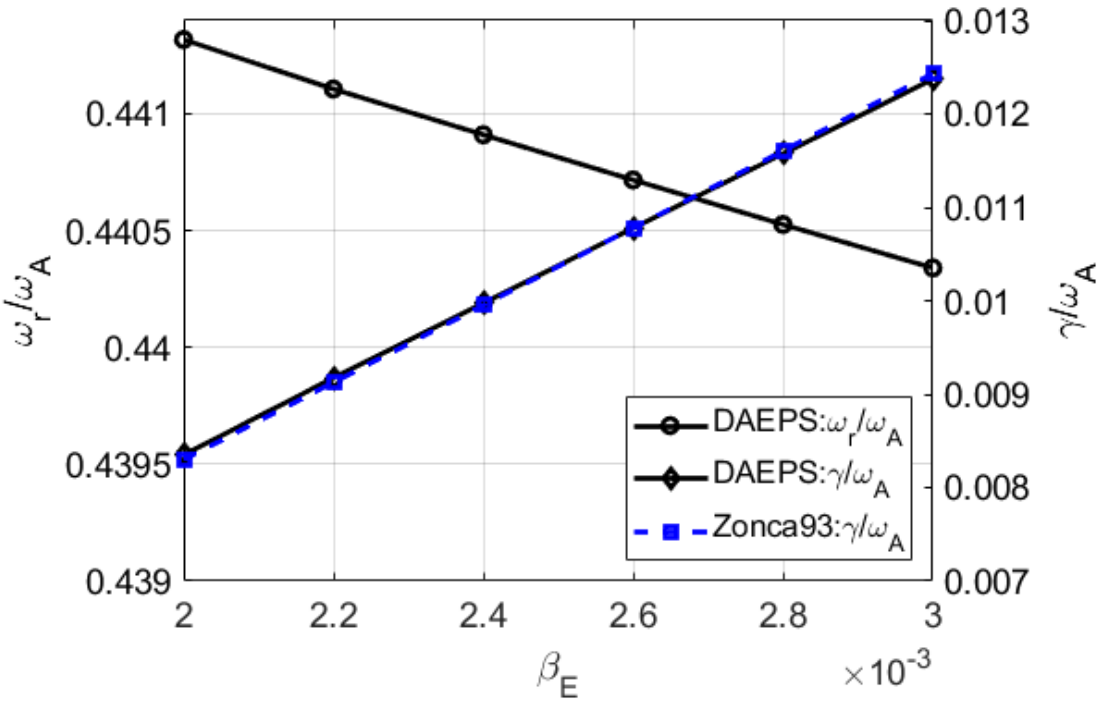

(b)

Figure 6: The eigen frequency of EP induced TAE varies with β_E (a) The TAE frequency and growth rate from DAEPS with FOW and FLR effects. (b) The TAE frequency and growth rate from DAEPS and theory without FOW and FLR effects.

VI. Conclusion and Discussion

In this paper, we developed a non-perturbative eigenvalue code DAEPS for the drift Alfvén energetic particle stability, and benchmarked the code with theory and other numerical codes on the instabilities involving circulating particle dynamics and MHD behavior, e.g., KBM, BAE and EP induced TAE, and Alfvén continuum. In the DAEPS model equations, we take the ideal MHD approximation for the background plasma, and keep the EP contribution in the kinetic compression (KC). We discussed in detail the numerical method employed in DAEPS, which uses cubic B-spline finite elements with special treatment near the computational boundary to deal with the Dirichlet or Neumann boundary condition as required by physics. We implemented a reduced KC term in the DAEPS code to accelerate the calculation of the eigen frequency, growth rate and asymptotic behavior for BAE/KBM dozens of times faster than using the complete KC term without losing accuracy. This makes DAEPS a practically useful toolkit for the experimentalists to study Alfvén instabilities with kinetic effects. The DAEPS result suggests that the effects of FOW and FLR can stabilize the BAE and TAE modes by suppressing the wave-particle resonance. In the DAEPS model equations, the asymptotic behavior of the mode structure is properly handled. Thus the DAEPS code can calculate marginally unstable or damping modes as well as continuous spectrum, which is absent from other codes; for unstable modes, the requirement of computational domain is reduced to save computational resources substantially. Furthermore, the DAEPS model equations satisfy the GFLDR equation automatically, which is capable of locating the essential Alfvénic physics and EP behaviors. The trapped particle contribution is ignored temporarily in this paper for simplicity and will be included in a future paper. In addition, the experimental equilibrium and profiles will be included in the DAEPS code as well.

ACKNOWLEDGEMENT

One of the authors, Y. Li would like to thank Professor L. Chen, F. Zonca, and Z.

Qiu, for useful discussions.

REFERENCES

[1] Vlad, G., Zonca, F., Briguglio, S. (2008). "Dynamics of Alfvén waves in tokamaks." La Rivista del Nuovo Cimento 22(7): 1-97.

[2] Wang, X., Briguglio, S., Lauber, Ph, Fusco, V., Zonca, F. (2016). "Structure of wave-particle resonances and Alfvén mode saturation." Physics of Plasmas 23(1).

[3] Wang, X., Zonca, F., Chen, L. (2010). "Theory and simulation of discrete kinetic beta induced Alfvén eigenmode in tokamak plasmas." Plasma Physics and Controlled Fusion 52(11).

[4] Chen, Yang, Parker, Scott E., Lang, J., Fu, G. Y.. (2010). "Linear gyrokinetic simulation of high-n toroidal Alfvén eigenmodes in a burning plasma." Physics of Plasmas 17(10).

[5] Ma, Ruirui, Chavdarovski, Ilija, Ye, Gaoxiang, Wang, Xin (2014). "Linear dispersion relation of beta-induced Alfvén eigenmodes in presence of anisotropic energetic ions." Physics of Plasmas 21(6).

[6] Zhang, H. S., Lin, Z., Holod, I., Wang, X., Xiao, Y., Zhang, W. L. (2010). "Gyrokinetic particle simulation of beta-induced Alfvén eigenmode." Physics of Plasmas 17(11).

[7] Qi, Longyu, Dong, J. Q., Bierwage, A., Lu, Gaimin, Sheng, Z. M. (2013). "Thermal ion effects on kinetic beta-induced Alfvén eigenmodes excited by energetic ions." Physics of Plasmas 20(3).

[8] Chu, M. S., Greene, J. M., Lao, L. L., Turnbull, A. D., Chance, M. S. (1992). "A numerical study of the high-nshear Alfvén spectrum gap and the high-ngap mode." Physics of Fluids B: Plasma Physics 4(11): 3713-3721.

[9] Fu, G. Y. and J. W. Van Dam (1989). "Excitation of the toroidicity-induced shear Alfvén eigenmode by fusion alpha particles in an ignited tokamak." Physics of Fluids B: Plasma Physics 1(10): 1949-1952.

[10] Chen, L. (1994). "Theory of Magnetohydrodynamic Instabilities Excited by Energetic Particles in Tokamaks." Physics of Plasmas 1(5): 1519-1522.

[11] Kusama, Y., Kimura, H., Ozeki, T., Saigusa, M., Kramer, G. J., Oikawa, T., Moriyama, S., Nemoto, M., Fujita, T., Tobita, K., Fu, G. Y., Nazikian, R., Cheng, C. Z. (1998). "Toroidal alfvén eigenmodes driven with ICRF accelerated protons in JT-60U negative shear discharges." Nuclear Fusion 38(8): 1215-1223.

[12] Heidbrink, W. W., Ruskov, E., Carolipio, E. M., Fang, J., van Zeeland, M. A., James, R. A. (1999). "What is the “beta-induced Alfvén eigenmode?”." Physics of Plasmas 6(4): 1147-1161.

[13] Chen, W., Ding, X. T., Yang, Q. W., Liu, Y., Ji, X. Q., Zhang, Y. P., Zhou, J., Yuan, G. L., Sun, H. J., Li, W.,

Zhou, Y., Huang, Y., Dong, J. Q., Feng, B. B., Song, X. M., Shi, Z. B., Liu, Z. T., Song, X. Y., Li, L. C., Duan, X. R., Liu, Y., Hl- A. team (2010). "beta-induced Alfven eigenmodes destabilized by energetic electrons in a Tokamak plasma." Phys Rev Lett 105(18): 185004.

[14] Heidbrink, W. W. (2008). "Basic physics of Alfvén instabilities driven by energetic particles in toroidally confined plasmas." Physics of Plasmas 15(5).

[15] Chen, L. and F. Zonca (2016). "Physics of Alfvén waves and energetic particles in burning plasmas." Reviews of Modern Physics 88(1).

[16] Zonca, F. (1993). "Alfvenic Instabilities Driven by Energetic Alpha-Particles." Plasma Physics and Controlled Fusion 35(SB): B307-B317.

[17] Cheng, C. Z., Chen, Liu, Chance, M. S. (1985). "High-n ideal and resistive shear Alfvén waves in tokamaks." Annals of Physics 161(1): 21-47.

[18] Hou, Yawei, Zhu, Ping, Kim, Charlson C., Hu, Zhaoqing, Zou, Zhihui, Wang, Zhengxiong (2018). "NIMROD calculations of energetic particle driven toroidal Alfvén eigenmodes." Physics of Plasmas 25(1).

[19] Briguglio, S., Vlad, G., Zonca, F., Kar, C. (1995). "Hybrid magnetohydrodynamic-gyrokinetic simulation of toroidal Alfvén modes." Physics of Plasmas 2(10): 3711-3723.

[20] Todo, Y. and T. Sato (1998). "Linear and nonlinear particle-magnetohydrodynamic simulations of the toroidal Alfvén eigenmode." Physics of Plasmas 5(5): 1321-1327.

[21] Konies, A., Briguglio, S., Gorelenkov, N., Feher, T., Isaev, M., Lauber, P., Mishchenko, A., Spong, D. A., Todo, Y., Cooper, A., Hatzky, R., Kleiber, R., Borchardt, M., Vlad, G., Biancalani, A., Bottino, A., ITPA EP TG (2018). "Benchmark of gyrokinetic, kinetic MHD and gyrofluid codes for the linear calculation of fast particle driven TAE dynamics." Nuclear Fusion 58(12).

[22] Zhu, J., Ma, Z. W., Wang, S. (2016). "Hybrid simulations of Alfvén modes driven by energetic particles." Physics of Plasmas 23(12).

[23] Biancalani, A., Bottino, A., Briguglio, S., Könies, A., Lauber, Ph, Mishchenko, A., Poli, E., Scott, B. D., Zonca, F. (2016). "Linear gyrokinetic particle-in-cell simulations of Alfvén instabilities in tokamaks." Physics of Plasmas 23(1).

[24] Mishchenko, Alexey, Könies, Axel, Hatzky, Roman (2009). "Global particle-in-cell simulations of fast-particle effects on shear Alfvén waves." Physics of Plasmas 16(8).

[25] Bierwage, A., Chen, L., Zonca, F. (2010). "Pressure-gradient-induced Alfvén eigenmodes: I. Ideal MHD and finite ion Larmor radius effects." Plasma Physics and Controlled Fusion 52(1): 015004.

[26] Hirose, A. and M. Elia (2002). "Integral-equation analysis of the kinetic-ballooning modes in tokamaks." Canadian Journal of Physics 80(12): 1517-1523.

[27] Xie, H. S., Lu, Z. X., Li, B. (2018). "Kinetic ballooning mode under steep gradient: High order eigenstates and mode structure parity transition." Physics of Plasmas 25(7).

[28] Rewoldt, G. (1982). "Electromagnetic kinetic toroidal eigenmodes for general magnetohydrodynamic equilibria." Physics of Fluids 25(3): 480.

[29] Zonca, F. and L. Chen (2014). "Theory on excitations of drift Alfvén waves by energetic particles. II. The general fishbone-like dispersion relation." Physics of Plasmas 21(7): 072121.

[30] Zonca, F. and L. Chen (2014). "Theory on excitations of drift Alfvén waves by energetic particles. I. Variational formulation." Physics of Plasmas 21(7): 072120.

[31] Lu, Z. X., Zonca, F., Cardinali, A. (2012). "Theoretical and numerical studies of wave-packet propagation in tokamak plasmas." Physics of Plasmas 19(4).

[32] Zonca, Fulvio, Chen, Liu, Santoro, Robert A. (1996). "Kinetic theory of low-frequency Alfvén modes in tokamaks." Plasma Physics and Controlled Fusion 38(11): 2011-2028.

[33] Connor, J. W., Hastie, R. J., Taylor, J. B. (1978). "Shear, Periodicity, and Plasma Ballooning Modes." Physical Review Letters 40(6): 396-399.

[34] Tsai, S. T. and L. Chen (1993). "Theory of Kinetic Ballooning Modes Excited by Energetic Particles in Tokamaks." Physics of Fluids B-Plasma Physics 5(9): 3284-3290.

[35] Falessi, Matteo Valerio, Carlevaro, Nakia, Fusco, Valeria, Vlad, Gregorio, Zonca, Fulvio (2019). "Shear Alfvén and acoustic continuum in general axisymmetric toroidal geometry." Physics of Plasmas 26(8).

[36] Jardin S C . "Computational Methods in Plasma Physics". CRC Press, Inc. 2010.

[37] Genz, A. C. and A. A. Malik (1980). "Remarks on algorithm 006: An adaptive algorithm for numerical integration over an N-dimensional rectangular region." Journal of Computational and Applied Mathematics 6(4): 295-302.

[38] Berntsen, Jarle, Espelid, Terje O., Genz, Alan (1991). "An adaptive algorithm for the approximate calculation of multiple integrals." ACM Transactions on Mathematical Software 17(4): 437-451.

[39] Zonca, F. and L. Chen (1993). "Theory of continuum damping of toroidal Alfvén eigenmodes in finite - β tokamaks." Physics of Fluids B: Plasma Physics 5(10): 3668-3690.

[40] Xie, H. S. and Y. Xiao (2015). "Parallel equilibrium current effect on existence of reversed shear Alfvén eigenmodes." Physics of Plasmas 22(2).